Photoacoustic imaging at 1064 nm wavelength with exogenous contrast agents

Paul Kumar Upputuri, Yuyan Jiang, Kanyi Pu and Manojit Pramanik*
School of Chemical and Biomedical Engineering, Nanyang Technological University, Singapore 637459

ABSTRACT

Photoacoustic (PA) imaging is a promising imaging modality for both preclinical research and clinical practices. Laser wavelengths in the first near infrared window (NIR-I, 650-950 nm) have been widely used for photoacoustic imaging. As compared with NIR-I window, scattering of photons by biological tissues is largely reduced in the second NIR (NIR-II) window, leading to enhanced imaging fidelity. However, the lack of biocompatible NIR-II absorbing exogenous agents prevented the use of this window for in vivo imaging. In recent years, few studies have been reported on photoacoustic imaging in NIR-II window using exogenous contrast agents. In this work, we discuss the recent work on PA imaging using 1064 nm wavelength, the fundamental of Nd:YAG laser, as an excitation wavelength. The PA imaging at 1064 nm is advantageous because of the low and homogeneous signal from tissue background, enabling high contrast in PA imaging when NIR-II absorbing contrast agents are employed.

***Keyword*:** photoacoustic imaging, contrast agent, in vivo imaging, second near-infrared window.

1. INTRODUCTION

Photoacoustic tomography (PAT) is a promising non-ionizing hybrid imaging modality combining high optical contrast and ultrasonic resolution for both preclinical and clinical applications.[1-3] In PAT a short laser pulse irradiates the tissue. Due to absorption of incident energy by the tissue chromophores (such as melanin, red blood cells, water etc.), there is a local temperature rise, which in turn produces pressure waves emitted in the form of acoustics waves. A wideband ultrasound transducer receives the photoacoustic signal outside the tissue boundary. PA signals are collected at different locations around the tissue boundary. Generally, circular scanning geometry in orthogonal excitation mode is preferred for deep tissue imaging. Reconstruction techniques are used to map the initial pressure rise within the tissue from the measured PA signals. PAI has several merits compared with pure optical and pure ultrasonic imaging modalities. Four types of PAI systems have been reported: (i) photoacoustic tomography (PAT) or photoacoustic computed tomography (PACT),[4] (ii) photoacoustic microscopy (PAM),[5-8] (iii) photoacoustic endoscopy (PAE),[9, 10] and (iv) photoacoustic nanoscopy (PAN).[11-15]

Usually, PAT systems use near-infrared (NIR) light with the wavelengths ranging from 650 to 950 nm (first NIR window, NIR-I) for deep tissue imaging.[16-22] There are numerous photoacoustic contrast agents in the NIR-I window to aid high contrast functional photoacoustic imaging.[23-29] Recent studies on fluorescence imaging have identified a new imaging window termed as the second NIR (NIR-II) window (1000-1700 nm).[30, 31] As compared with the NIR-I window, fluorescence imaging in the NIR-II window affords reduced photon scattering in biological tissues and lower tissue background, leading to quality imaging.[32, 33] Due to these advantages, it is envisioned that PA imaging in the NIR-II window could bring about further improved imaging performance. The advantages of using 1064 nm for PA imaging: (i) due to the relatively lower photon energy at longer wavelength, the maximum permissible exposure (MPE) increases with the laser wavelength and the MPE for skin is 100 mJ/cm^2 for 1064 nm laser, which is 25 mJ/cm^2 for 750 nm laser,[34] (ii) commercial availability of cheaper, and more compact 1064 nm Nd: YAG laser (additionally OPO is required for NIR-I window imaging), (iii) the output of Nd:YAG 1064 laser has good beam quality- allows uniform illumination without using optical diffuser, low divergence – it is easy to deliver beam though free space optics, very low power

* Email: manojit@ntu.edu.sg

Photons Plus Ultrasound: Imaging and Sensing 2018, edited by Alexander A. Oraevsky, Lihong V. Wang, Proc. of SPIE Vol. 10494, 104943K · © 2018 SPIE · CCC code: 0277-786X/18/$18 · doi: 10.1117/12.2287084

fluctuations – measurements are reproducible. The key challenges to fulfil 1064 nm PA imaging include: (i) the blood has relatively low absorption at 1064 nm, (ii) 1064 nm is invisible to human eyes, so IR cards / viewers may be required for alignment, (iii) exogenous agent with strong 1064 nm-absorption is required for contrast enhancement. Few exogenous agents that can absorb wavelength in the NIR-II window are: copper sulfide nanoparticles,[35] silver nanoplates,[36] gold nanorods,[37] and phosphorous phthalocyanine.[38] Semiconducting polymer nanoparticles (SPNs) have been utilized for NIR-II fluorescence imaging.[39] SPNs are mainly composed of organic semiconducting polymers with highly electron-delocalized backbones, and have formed a new class of optical agents.[40] The SPNs can efficiently convert photon energy into heat, permitting photothermal cancer therapy,[41] and photoacoustic imaging of tumor,[42] lymph node,[43] and biomarkers in living animals.[44] Particularly, SPNs often possess higher absorption and photothermal conversion efficiencies as compared with other inorganic nanoparticles such as gold nanorods and carbon nanotubes.[43] In this paper we will demonstrate SPN as an efficient contrast agent for PA imaging at 1064 nm. More details on the synthesis and characterization of NIR-II absorbing SPN (SPN-II) based contrast agent can be found in Ref.[45] SPN-II had a broadband absorption spectrum ranging from visible to NIR II region with the maximum peak at 1253 nm. Here we discuss about the experimental PAT system, deep-tissue imaging at 1064 nm (NIR-II), and finally we compare deep-tissue images obtained at 1064 nm and 750 nm.

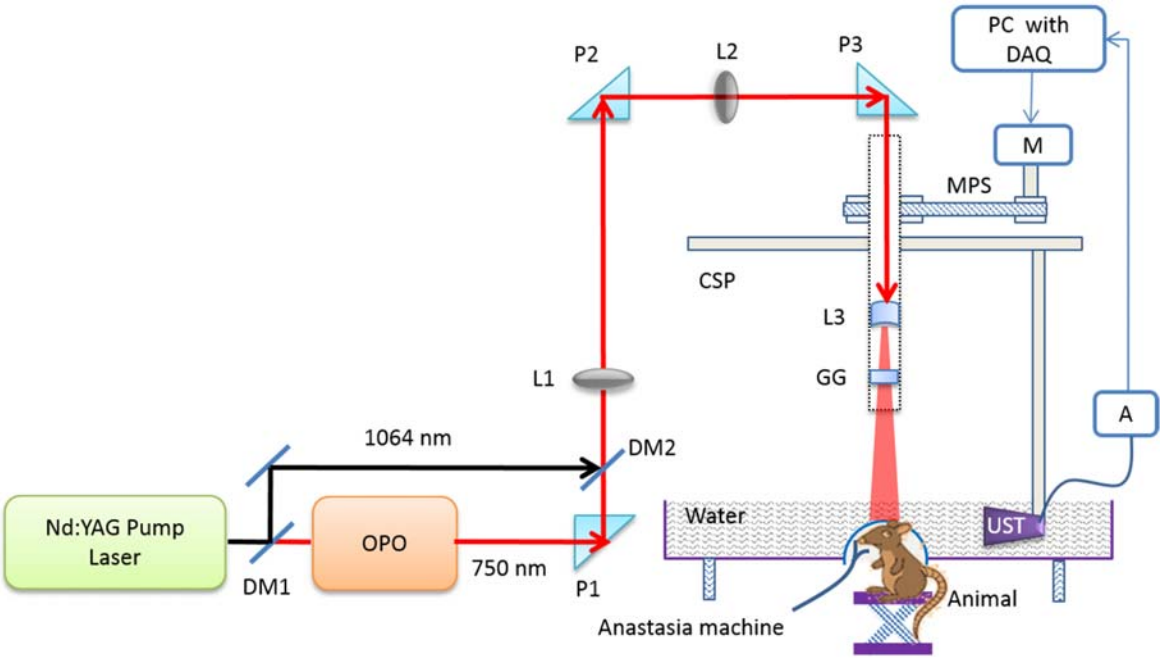

Fig. 1. Schematic illustration of Nd:YAG/OPO PAT system: DM - dichromic mirror, P - antireflection-coated right angle prism, MPS - motor pulley system, CSP - circular scanning plate, (L1,L2) convex lens, L3 - concave lens, GG - ground glass, DAQ - data acquisition card, M - motor, A - ultrasound signal amplifier, UST - ultrasound transducer.

2. PHOTOACOUSTIC TOMOGRAPHY SYSTEM FOR SECOND WINDOW IMAGING

The Nd:YAG/OPO based PAT system is shown in Fig. 1. The excitation laser consists an optical parametric oscillator (Continuum, Surelite OPO) system pumped by a 532 nm Nd:YAG laser (Continuum, Surelite Ex). The Nd:YAG laser generates it fundamental at 1064 nm and its second harmonic at 532 nm. A dichroic mirror (DM1) was used to separate 1064 nm from 532 nm. The OPO was pumped by the 532 nm beam. The OPO generated 5 ns duration pulses at 10 Hz repetition rate with wavelength tunable from 680 nm to 2500 nm. The 1064 nm from Nd:YAG pump laser, and 750 nm from OPO were guided by the two convex lenses (L1 and L2) to the scanner, and then expanded using a concave lens (L3). A ground glass (GG) is used to make the laser beam more uniform. The laser fluence on tissue surface was ~5

mJ/cm^2 which is within the ANSI maximum permissible exposer (MPE). The PA signal generated by the sample was received by a non-focused transducer (V323-SU/2.25 MHz, Olympus NDT) with a 13 mm active area and 70% nominal bandwidth. The transducer was driven by a computer-controlled stepper motor (SM) to continuously move in a circular motion. The PA signals were subsequently amplified, band-pass filtered by an ultrasound pulser/receiver unit (AU), (Olympus NDT, 5072PR) and then digitized and recorded by the PC with a DAQ (data acquisition) card (25 Ms/s, GaGe, compuscope 4227). After data collection a simple delay-and-sum reconstruction algorithm[46, 47] was used to form the cross-sectional photoacoustic images of the sample.

3. EXPERIMENTAL RESULTS

The PA spectra of SPN-II and water are shown in Figure 2. SPN-II exhibited strong PA signals in both NIR I and II windows. The SPN-II showed nearly identical PA amplitudes at 750 nm and 1064 nm. So we used these two wavelengths to compare deep imaging capabilities of NIR-I and NIR-II windows. Note that the PA amplitude of water at 1064 nm was lower than that at 750 nm, implying the lower background noise in the NIR-II window. Linear correlation between the concentration of SPN-II and PA amplitudes at 750 or 1064 nm was observed, indicating the applicability for signal quantification.

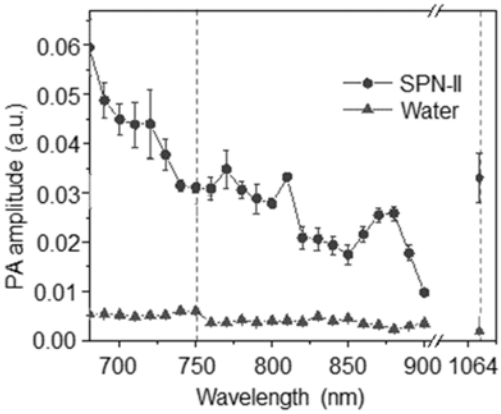

Fig. 2. Photoacoustic spectra of SPN-II (200 μg/mL) and water. Error bars indicate standard deviations of 10 separate measurements.

To validate the advantage of SPN-II for PA imaging in the NIR II window, deep tissue imaging was conducted on a homemade two-wavelength PA imaging system with the ability to image at both 750 and 1064 nm (Figure 1). The solutions of SPN-II with 4 different concentrations were embedded in an agar gel phantom and was placed under chicken breast tissues with different thicknesses. To compare NIR-I and NIR-II imaging in terms of imaging depth, PA images were acquired at both 750 and 1064 nm with the identical laser energy density of ~5 mJ/cm^2. At the highest concentration (1 mg/mL, spot c4), the PA signals were detectable in both NIR-I and NIR-II window at the tissue depth up to 3 cm. We found that the signal-to-noise ratio (SNR) for NIR-II imaging was higher than that for NIR-I imaging at all depths. At 3 cm-depth, the 0.5 mg/mL spot c3 is visible in NIR-II but not in NIR-I window. The enhanced SNR for NIR-II PA imaging should be mainly attributed to the significantly decreased background signals in the NIR-II relative to NIR-I.[36] Due to the relatively lower photon energy at longer wavelength, the maximum permissible exposure (MPE) increases with the laser wavelength and the MPE for skin is 100 mJ/cm^2 for 1064 nm laser, which was 25 mJ/cm^2 for 750 nm laser. With the laser power of 56 mJ/cm^2, PA imaging at 1064 nm has been reported to reach ~11.6 cm in chicken breast tissue.[38]

4. CONCLUSIONS

A SPN-based PA contrast agent that had broadband absorption in both NIR-I and NIR-II windows was designed and synthesized, discussed in detail in Ref.[45] The SPN-II had nearly identical PA amplitudes at 750 and 1064 nm, hence enabled direct comparison between NIR-I and NIR-II PA imaging. The SPN-II resulted PA images acquired at 1064 nm could exhibit 1.4-times higher SNR than that at 750 nm at the tissue depth of 3 cm, mainly owing to the decreased background PA signals of biological tissue at 1064 nm. The application of SPN-II for *in vivo* 1064 nm PA imaging was demonstrated in imaging of brain vasculature in living rats, discussed in detail in Ref.[45] The study proved that the SNR of 1064 nm PA imaging is higher relative to that of 750 nm PA imaging, this could be further enhanced by increasing the laser power due to the higher MPE at 1064 nm. We believe that this study provides the clear evidence to support that 1064 nm (NIR-II) is an optimal wavelength for enhancing the contrast of PA imaging compared to 750 nm (NIR-I).

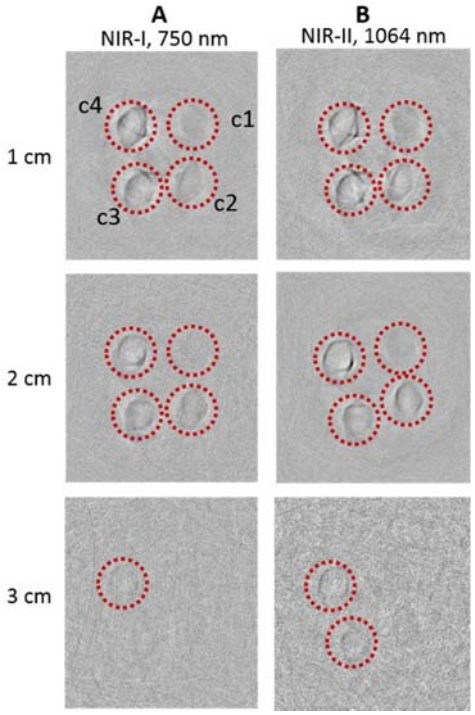

Fig. 3. Deep tissue *in vitro* imaging. (A) Two-dimensional PA images of the agar gel phantom containing SPN-II solutions acquired in both NIR windows at different depths. Left: NIR-I window (750 nm), Right: NIR-II window (1064 nm). Same energy density ~5.5 mJ/cm2 was used at 750 nm and 1064 nm. The agar gel phantom containing SPN-II dots with different concentrations (c1-c4: 0.05, 0.2, 0.5 and 1 mg/mL, respectively).

ACKNOWLEDGMENT

The authors would like to acknowledge the financial support from the Singapore Ministry of Health's National Medical Research Council (NMRC/OFIRG/0005/2016: M4062012), and the start-up Grant by Nanyang Technological University (SUG: M4081627). Authors have no relevant financial interests in the manuscript and no other potential conflicts of interest to disclose.

REFERENCES

[1] P. K. Upputuri, and M. Pramanik, "Recent advances toward preclinical and clinical translation of photoacoustic tomography: a review," Journal of Biomedical Optics, 22(4), 041006 (2017).

[2] P. K. Upputuri, K. Sivasubramanian, C. S. K. Mark *et al.*, "Recent developments in vascular imaging techniques in tissue engineering and regenerative medicine," BioMed Research International, 2015, 9 (2015).
[3] L. V. Wang, "Multiscale photoacoustic microscopy and computed tomography," Nature Photonics, 3(9), 503-509 (2009).
[4] L. Li, L. Zhu, C. Ma *et al.*, "Single-impulse panoramic photoacoustic computed tomography of small-animal whole-body dynamics at high spatiotemporal resolution," Nature Biomedical Engineering, 1, 0071 (2017).
[5] M. Moothanchery, R. Z. Seeni, C. Xu *et al.*, "In vivo studies of transdermal nanoparticle delivery with microneedles using photoacoustic microscopy," Biomedical Optics Express, 8(12), 5483-5492 (2017).
[6] M. Moothanchery, A. Sharma, and M. Pramanik, "Switchable Acoustic and Optical Resolution Photoacoustic Microscopy for in vivo small-animal blood vasculature imaging," Journal of Visualized Experiments(124), e55810 (2017).
[7] M. Moothanchery, and M. Pramanik, "Performance Characterization of a Switchable Acoustic and Optical Resolution Photoacoustic Microscopy System," Sensors, 17(2), 357 (2017).
[8] S.-L. Chen, L. J. Guo, and X. Wang, "All-optical photoacoustic microscopy," Photoacoustics, 3(4), 143-150 (2015).
[9] H. He, G. Wissmeyer, S. V. Ovsepian *et al.*, "Hybrid optical and acoustic resolution optoacoustic endoscopy," Optics Letters, 41(12), 2708 (2016).
[10] J. M. Yang, K. Maslov, H. C. Yang *et al.*, "Photoacoustic endoscopy," Optics Letters, 34(10), 1591-93 (2009).
[11] P. K. Upputuri, M. Krishnan, and M. Pramanik, "Microsphere enabled sub-diffraction limited optical-resolution photoacoustic microscopy: a simulation study," Journal of Biomedical Optics, 22(4), 045001 (2017).
[12] P. K. Upputuri, and M. Pramanik, "Microsphere-aided optical microscopy and its applications for super-resolution imaging," Optics Communications, 404, 32-41 (2017).
[13] P. K. Upputuri, Z.-B. Wen, Z. Wu *et al.*, "Super-resolution photoacoustic microscopy using photonic nanojets: a simulation study," Journal of Biomedical Optics, 19(11), 116003 (2014).
[14] A. Danielli, K. Maslov, A. Garcia-Uribe *et al.*, "Label-free photoacoustic nanoscopy," Journal of Biomedical Optics, 19(8), 086006 (2014).
[15] J. Yao, L. Wang, C. Li *et al.*, "Photoimprint Photoacoustic Microscopy for Three-Dimensional Label-Free Subdiffraction Imaging," Physical Review Letters, 112(1), 014302 (2014).
[16] P. K. Upputuri, and M. Pramanik, "Dynamic in vivo imaging of small animal brain using pulsed laser diode-based photoacoustic tomography system," Journal of Biomedical Optics, 22(9), 090501 (2017).
[17] P. K. Upputuri, V. Periyasamy, S. K. Kalva *et al.*, "A High-performance compact photoacoustic tomography system for in vivo small-animal brain imaging," Journal of Visualized Experiments(124), e55811 (2017).
[18] Q. Chen, X. Liu, J. Chen *et al.*, "A Self‐Assembled Albumin‐Based Nanoprobe for In Vivo Ratiometric Photoacoustic pH Imaging," Advanced Materials, 27(43), 6820-6827 (2015).
[19] P. K. Upputuri, and M. Pramanik, "Performance characterization of low-cost, high-speed, portable pulsed laser diode photoacoustic tomography (PLD-PAT) system," Biomedical Optics Express, 6(10), 4118-29 (2015).
[20] P. K. Upputuri, and M. Pramanik, "Pulsed laser diode based optoacoustic imaging of biological tissues," Biomedical Physics & Engineering Express, 1(4), 045010-7 (2015).
[21] V. Ntziachristos, and D. Razansky, "Molecular Imaging by Means of Multispectral Optoacoustic Tomography (MSOT)," Chemical Reviews, 110(5), 2783-2794 (2010).
[22] S. Manohar, S. E. Vaartjes, J. C. G. v. Hespen *et al.*, "Initial results of in vivo non-invasive cancer imaging in the human breast using near-infrared photoacoustics," Optics Express, 15(19), 12277-12285 (2007).
[23] Y. Gawale, N. Adarsh, S. K. Kalva *et al.*, "Carbazole Linked NIR Aza-BODIPY Dyes as Triplet Sensitizers and Photoacoustic Contrast Agents for Deep Tissue Imaging," Chemistry - A European Journal, 23(27), 6570-6578 (2017).
[24] K. Sivasubramanian, M. Mathiyazhakan, C. Wiraja *et al.*, "Near Infrared light-responsive liposomal contrast agent for photoacoustic imaging and drug release applications," Journal of Biomedical Optics, 22(4), 041007 (2017).
[25] S. Huang, P. K. Upputuri, H. Liu *et al.*, "A dual-functional benzobisthiadiazole derivative as an effective theranostic agent for near-infrared photoacoustic imaging and photothermal therapy," Journal of Materials Chemistry B, 4(9), 1696-1703 (2016).

[26] D. Pan, M. Pramanik, S. A. Wickline *et al.*, "Recent advances in colloidal gold nanobeacons for molecular photoacoustic imaging," Contrast Media and Molecular Imaging, 6(5), 378-88 (2011).
[27] D. Pan, M. Pramanik, A. Senpan *et al.*, "A facile synthesis of novel self-assembled gold nanorods designed for near-infrared imaging," Journal of Nanoscience and Nanotechnology, 10(12), 8118-8123 (2010).
[28] C. Kim, C. Favazza, and L. V. Wang, "In vivo photoacoustic tomography of chemicals: high-resolution functional and molecular optical imaging at new depths," Chemical Reviews, 110(5), 2756-82 (2010).
[29] M. Pramanik, M. Swierczewska, D. Green *et al.*, "Single-walled carbon nanotubes as a multimodal-thermoacoustic and photoacoustic-contrast agent," Journal of Biomedical Optics, 14(3), 034018 (2009).
[30] S. Zhu, Q. Yang, A. L. Antaris *et al.*, "Molecular imaging of biological systems with a clickable dye in the broad 800-to 1,700-nm near-infrared window," Proceedings of the National Academy of Sciences, 201617990 (2017).
[31] A. L. Antaris, H. Chen, K. Cheng *et al.*, "A small-molecule dye for NIR-II imaging," Nature materials, 15(2), 235-242 (2016).
[32] G. Hong, A. L. Antaris, and H. Dai, "Near-infrared fluorophores for biomedical imaging," Nature Biomedical Engineering, 1, 0010 (2017).
[33] A. M. Smith, M. C. Mancini, and S. Nie, "Second window for in vivo imaging," Nature nanotechnology, 4(11), 710-711 (2009).
[34] [American National Standard for Safe Use of Lasers ANSI Z136.1-2007 (American National Standards Institute, Inc., New York, NY, 2007)].
[35] G. Ku, M. Zhou, S. Song *et al.*, "Copper sulfide nanoparticles as a new class of photoacoustic contrast agent for deep tissue imaging at 1064 nm," ACS Nano, 6(8), 7489-96 (2012).
[36] K. Homan, S. Kim, Y.-S. Chen *et al.*, "Prospects of molecular photoacoustic imaging at 1064 nm wavelength," Optics Letters, 35(15), 2663-2665 (2010).
[37] Y.-S. Chen, K. Homan, D. Xu *et al.*, "Feasibility of Contrast-Enhanced Photoacoustic Liver Imaging at a Wavelength of 1064 nm," OSA Technical Digest. BM2B.7.
[38] Y. Zhou, D. Wang, Y. Zhang *et al.*, "A Phosphorus Phthalocyanine Formulation with Intense Absorbance at 1000 nm for Deep Optical Imaging," Theranostics, 6(5), 688-697 (2016).
[39] C.-T. Kuo, A. M. Thompson, M. E. Gallina *et al.*, "Optical painting and fluorescence activated sorting of single adherent cells labelled with photoswitchable Pdots," Nature Communications, 7, 11468 (2016).
[40] Y. Wang, S. Li, L. Liu *et al.*, "Conjugated Polymer Nanoparticles to Augment Photosynthesis of Chloroplasts," Angewandte Chemie, (2017).
[41] H. Zhu, Z. Lai, Y. Fang *et al.*, "Ternary Chalcogenide Nanosheets with Ultrahigh Photothermal Conversion Efficiency for Photoacoustic Theranostics," Small, 13(16), 1604139-n/a (2017).
[42] C. Xie, P. K. Upputuri, X. Zhen *et al.*, "Self-quenched semiconducting polymer nanoparticles for amplified in vivo photoacoustic imaging," Biomaterials, 119, 1-8 (2017).
[43] K. Pu, A. J. Shuhendler, J. V. Jokerst *et al.*, "Semiconducting polymer nanoparticles as photoacoustic molecular imaging probes in living mice," Nat Nano, 9(3), 233-239 (2014).
[44] J. Zhang, X. Zhen, P. K. Upputuri *et al.*, "Activatable Photoacoustic Nanoprobes for In Vivo Ratiometric Imaging of Peroxynitrite," Advanced Materials, (2016).
[45] Y. Jiang, P. K. Upputuri, C. Xie *et al.*, "Broadband Absorbing Semiconducting Polymer Nanoparticles for Photoacoustic Imaging in Second Near-Infrared Window," Nano Letters, (2017).
[46] S. K. Kalva, and M. Pramanik, "Use of acoustic reflector to make compact photoacoustic tomography system," Journal of Biomedical Optics, 22(2), 026009 (2017).
[47] S. K. Kalva, and M. Pramanik, "Experimental validation of tangential resolution improvement in photoacoustic tomography using a modified delay-and-sum reconstruction algorithm," Journal of Biomedical Optics, 21(8), 086011 (2016).